Harvesting Ambient RF Energy Efficiently With Optimal Angular Coverage

E. Vandelle, D. Bui, T.P. Vuong, G. Ardila, K. Wu, S. Hemour

Harvesting Ambient RF Energy Efficiently with Optimal Angular Coverage

E. Vandelle, Student Member, IEEE, D.H.N. Bui, Student Member, IEEE, T.P. Vuong, Senior Member, IEEE, G. Ardila, K. Wu, Fellow, IEEE, S. Hemour, Senior Member, IEEE

***Abstract*— Ambient electromagnetic and RF energy is an ubiquitous energy resource that is found everywhere but difficult to harvest because of the time-varying orientation of incoming radiations and the low efficiency of RF rectifiers resulting from a low input power density operation. In response to these two challenges that come with the design of rectennas for ambient energy harvesting, this paper discusses a Figure-of-Merit to evaluate the rectenna performance that combines the rectification efficiency, the radiation efficiency, and the spherical coverage of the antenna. To illustrate this proposed Figure-of-Merit, a rectenna with a strengthen RF-to-DC efficiency and also a full spatial coverage is designed using beam-forming networks. The resulting system is demonstrated for a wireless sensor mounted on a pole. To maintain a reasonable size of the prototype, a miniaturization technique of a 4x4 Butler matrix is investigated, which allows for the reduction of the footprint of the Butler matrix by 2 compared to its classical microstrip design counterpart at 2.4 GHz. The overall rectification efficiency and DC power patterns are reported for the elevation plane of one multidirectional rectenna at 2.4 GHz for an incident power density of 0.45 µW.cm^{-2}. It is shown that the system can triple the DC output power compared to a 3-dipole counterpart occupying the same area. Furthermore, while the maximum harvesting capability at 1 µW.cm^{-2} does not exceed 28 π %.steradian in the literature, it reaches 43.6π %.steradian with the proposed demonstrator.**

***Index Terms*—ambient RF energy harvesting, harvesting capability, solid angle, beam forming network (BFN), miniaturized Butler matrix, rectenna, high gain, quasi-isotropic radiation, efficiency pattern.**

I. Introduction

The deployment of wireless sensor networks (WSNs) has led to the investigation of self-powered electronics with ambient energy harvesting to avoid maintenance cost and practical issues. Meanwhile, our urban areas have become ubiquitous radiofrequency (RF) environments subject to abundant ambient RF energy suitable for powering low duty cycle and low power wireless sensors. The harvesting of such an ambient energy requires the use of a rectifying antenna (rectenna) that captures RF power and converts it into DC or even required AC power. In most cases, the DC power is preferred because of its compatibility with the current electronic design and battery operation and the rectenna performance is usually evaluated through the RF to DC conversion efficiency. There are two issues in the design of an efficient far-field rectenna for ambient energy. The first one is a low rectification efficiency operation due to the low ambient RF power density at legacy communication frequencies: from 0.1 µW.cm^{-2} on average in urban areas [1] to some µW.cm^{-2} near WiFi routers [2] have been reported. The derivation of the RF-to-DC conversion efficiency of a single serial diode when operating at ambient power levels shows indeed that it is directly proportional to the input power [3]. Typically, no more than 17.5 % efficiency at -30 dBm and 4 % at -40 dBm have been reached with backward diodes [4]. The second issue is that the positioning of RF transmitter or the orientation of rectenna is usually unknown or time varying, leading to completely random angles of arrival of RF waves on the harvester [5]. Therefore, a well-designed ambient RF energy rectenna should not only operate in its high efficiency region but also be insensitive to the positioning of the energy source. In fact this is such a big challenge that the second point has been most of the time neglected in the literature.

Conventional rectenna designs with high gain compact antennas [6], [7] or antenna arrays [8], [9] have already been implemented to increase the received RF power. However, the directive nature of high gain antennas does not fulfil the requirement for the rectennas to be omnidirectional. At the same time, dipole rectennas have been commonly adopted, because of their quasi full spatial coverage of linearly polarized radiations [10]-[12] or other strategies like 3D structures with multiple inkjet-printed antennas covering different directions [13] have also been proposed to increase the spatial coverage. These antennas exhibit nonetheless a limited gain, coming up with a limited rectification efficiency. In an effort of strengthening the rectifier input power to a higher level, several sources of energy can be collected altogether and rectified by a single element. Thanks to the frequency and polarization diversity of the ambient energy, rectennas operating at different frequency bands [11]-[12], [14]-[18] or different polarizations [6], [15], [17] have been developed. In [19], RF and kinetic energies are efficiently added up to consequently improve the conversion efficiency of the diode. Yet, in the last cited scenarios, the improvement is limited to the case where the different sources are simultaneously collected. In fact, the combination of RF power conducted by antennas with high effective aperture is the most effective way to receive a sufficient power so that it is rectified with high efficiency when low power such as ambient cases is involved. That is why cumulating RF power combination and wide beam width radiation are now being explored like [20] or in [21] where a power combining rectenna array with a beam-forming matrix was proposed to increase both the received power and the beam width in the E-plane of the rectenna.

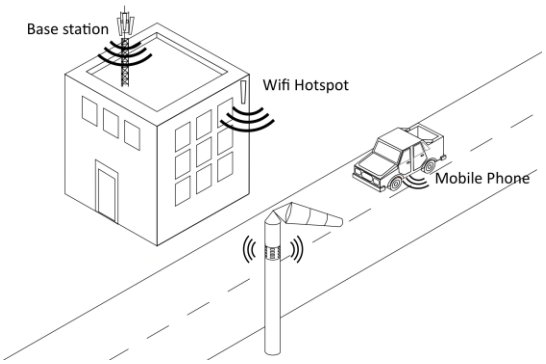

Fig. 1. Application example of the proposed rectenna. Positioned on a windsock pole, 5 vertical antenna arrays harvest with high gain upward and downward vertically polarized ambient RF radiation coming from base stations, wifi hotspot or mobile phones.

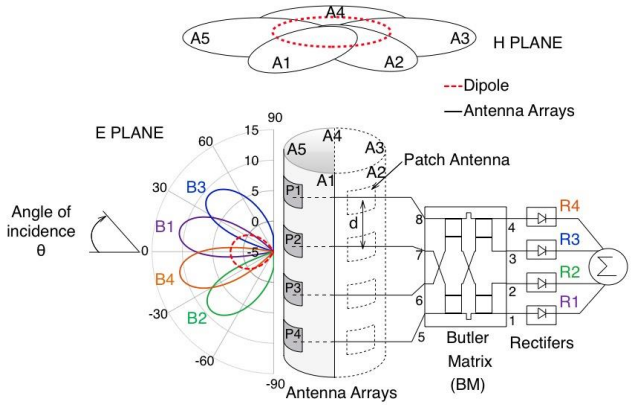

Fig. 2. Schetch of the linearly polarised RF power combining quasi-isotropic energy harvester and its radiation pattern in the E and H-planes. The radiation pattern is comparable to the radiation pattern of an omnidirectional electric dipole antenna vertically polarised but with 6 dB higher gain on average.

This paper proposes a novel Figure-of-Merit to evaluate the rectennas performance, called harvesting capability that considers not only the rectification efficiency but also the spatial coverage. The contribution of RF power combination in the performance of ambient energy harvesting rectenna is experimentally demonstrated and a solution to obtain RF power combination associated with a full spatial coverage is devised. To illustrate the proposed Figure-of-Merit, high gain antenna arrays with beam forming networks are designed to obtain a highly efficient rectenna with quasi-isotropic harvesting capability. A complete description of the system that has been first proposed in [22] is given here. An effort is furnished to reduce the system size and a cylindrical antenna array is prototyped to be mounted on a pole. The system is designed to scavenge energy from telecommunication radiations emitted from any location. Those radiations are usually found with vertical polarization even if subject to some reflection between transceivers. Hence, the radiation pattern of the proposed rectenna is comparable to the radiation pattern of a vertically polarized electric dipole antenna but with a 6 dB higher gain on average and wider beam width in the E-plane. As shown in Figure 1, the system could directly supply energy to a low duty cycle and low power sensor that captures information in a pole environment. Five vertical antenna arrays are equally positioned around the pole so that any direction in the magnetic field (H) plane is covered. A simple passive beam-forming network (BFN) allows for each vertical array to collect energy though high gain from different orientations over a 120° angle, thus optimizing the system size. In this way, RF radiation arriving from upward (base station, WiFi hotspots) or downward (mobile phones) can be harvested all around the pole. The proposed rectenna is shown in Figure 2. The BFN consists of a 4x4 Butler matrix (BM) that controls the phase of the incoming signals (at ports 5, 6, 7 and 8) to redirect them into one rectifier (R1, R2, R3 or R4) depending on the incoming beam's orientation (B1, B2, B3 or B4). The system allows the collection of RF energy with high gain multidirectional antenna arrays and through the power enhancement at the rectifier's inputs, the rectifiers operate efficiently for any position of the energy source.

Section II of this paper introduces the description of the harvesting capability of ambient energy harvesting rectennas and derives the harvesting capability of the proposed demonstrator. Section III presents the results of a miniaturized Butler matrix. In section IV, the quasi-isotropic radiation pattern of a cylindrical antenna array with BFNs is presented. Section V shows the measured efficiency and DC power patterns of one multidirectional rectenna functioning in the 2.4 GHz band. Finally, the sensitivity of the proposed rectenna is discussed in section VI and a comparison of state-of-the-art rectennas is given in section VII.

II. Harvesting Capability

A. Rectification Efficiency

The RF-to-DC conversion efficiency of a single diode rectifier under an optimal condition where the load R_L is equal to the junction resistance R_j of the diode is given by [3]

$$\eta_r = P_{RF}.B_o = P_{RF}.(\Re_I^2).\eta_{MN}{}^2.\left(\frac{\sqrt{R_j}}{2+2\omega_o^2 R_j R_s}\right)^2 \quad (1)$$

where P_{RF} is the RF power available at the rectifier input and B_o depends on the rectifier performance. $\Re_I$ is the current responsivity of the diode defined as the ratio between the output DC current for a 0-Ω load and the input RF power at the fundamental frequency f_o. $\Re_I$ is constant under low input power, low frequency and high load resistor, and depends only on the diode junction technology. η_{MN} represents the losses of the impedance matching network between the antenna and the diode, R_s is the series resistance of the diode and ω_o is the angular frequency. Equation (1) shows that the rectification efficiency of a single diode rectifier is proportional to the power available at the rectifier input that is the power captured by the antenna defined as

$$P_{RF} = S.A = S.\frac{\lambda_o^2}{4\pi}.|G(\theta,\phi)| \quad (2)$$

in which S is the power density at the antenna level and A the antenna effective aperture, generally defined at the maximum

radiation intensity. Thus $|G(\theta,\varphi)|$ is the magnitude of the maximum antenna gain at frequency f_o and λ_o is the wave-length in free space. As the rectification efficiency is proportional to the RF power captured by the antenna, the output DC power varies with the square of the input power. Hence equation (2) suggests that, for a given power density, high gain rectennas are more efficient and can deliver much more power than omnidirectional rectennas with lower gain.

B. Harvesting Capability of Ambient Energy Harvesting Rectennas

The improvement of the rectenna gain is classically possible only at the expense of the radiation beam width. That is why it is important not to omit the spatial coverage in the performance evaluation of rectennas for ambient RF energy harvesting. For this, the harvesting capability C_{harv} in %.steradian, introduced in [22], is used in this paper. It is defines as the product of the rectification efficiency $\eta_{r_{max}}$ and the solid angle Ω of the rectenna's radiation pattern. Note that, since the solid angle of a sphere is 4π, the maximum harvesting capability of a rectenna is 100π %.steradian.

$$C_{harv} = \eta_{r_{max}}.\Omega\ /4 \quad \text{[\%.steradian]} \quad (3)$$

The solid angle of antennas can be computed for directive and omnidirectional (in the H plane) radiation patterns with equations (4) and (5) respectively [23] where Θ_E and Θ_H are the half power beam widths (HPBW) in radians in the E and H planes of the rectenna radiation pattern. For rectangular patch antennas, the HPBWs can also be calculated from the antenna parameters [23].

$$\Omega \approx \Theta_E \Theta_H \quad (4)$$

$$\Omega \approx 4\pi\ /(-172.4 + 191\sqrt{0.818 + \frac{180}{\pi.\Theta_E}}) \quad (5)$$

C. Proposed Rectenna Harvesting Capability

The far-field complex gain pattern of a linear array of N antennas associated with a NxN Butler matrix results in N beams of different gains G_{B_i} and different orientations due to the phases between the antennas β_i fixed by the Butler matrix, i =1,…N. The gain of each beam can be expressed as in (6) in the spherical coordinates.

$$G_{B_i}(\theta,\phi) = \sum_{n=1}^{N} G_{Pn}(\theta,\phi).\left|A_n^i\right|.exp(j(n-1)(k_o d sin\theta cos\phi + \beta_i) \quad (6)$$

$G_{Pn}(\theta,\phi)$ is the active element gain of the nth antenna element, d is the inter-element spacing and $\left|A_n^i\right|$ is the magnitude of the excitation coefficient of the nth element. The maximum gain in the plane $\phi = 0$ is obtained when the phase of the active element gains plus the phase term $(n-1)(k_o d sin\theta)$ are cancelled out by the phase of the excitation coefficients. For each beam B_i, this occurs at a specific scan angle θ_o^i given by (7).

$$\theta_o^i = -\sin^{-1}(\frac{-\beta_i}{k_o d}) \quad (7)$$

Then, the maximum co-polar gain magnitude of one beam (in the E-plane) at $\phi = 0$ is given by (8).

$$\left|G_{B_i}(\theta,0)\right| = \left|\sum_{n=1}^{N}|G_{Pn}^{co}(\theta,0)|.\left|A_n^i\right|.exp(jk_o(n-1)d\,(sin(\theta) - sin(\theta_o^i))\right| \quad (8)$$

The proposed demonstrator is composed of 4x4 Butler matrices that give phase shifts β_i equal to 45°, -135°, 135° and -45° for i = 1, 2, 3 and 4, respectively. Then, the inter-element spacing $d = \lambda_o/2$ *i*n a 4-antennas array leads to 4 high gain beams, at the scan angles: $\theta_o^1 = 14°$, $\theta_o^2 = 48°$, $\theta_o^3 = -48°$, $\theta_o^4 = -14°$ respectively. From (1)-(4) and (8), we can now derive the harvesting capability of the demonstrator. When similar antennas are used, the RF power received by the rectifiers R_i of the demonstrator as well as their rectification efficiency can be multiplied by up to 4 compared to one rectifier with a single antenna. Then, because of the lower scanning losses at the scanning angles 14° and -14°, the maximum gain of the system is equal to $4 * \left|G_P^{co}(\theta_o^{1,4},0)\right|$. Furthermore, for each of the 5 antenna arrays, we have two directive centre beams with HPBWs $\Theta_{E1}\Theta_{H1}$ and two directive side beams with HPBWs $\Theta_{E2}\Theta_{H2}$, leading to a solid angle equivalent to $10 * (\Theta_{E1}\Theta_{H1} + \Theta_{E2}\Theta_{H2})$. Finally the harvesting capability of the proposed rectenna can be expressed as (9) where δ represents the losses introduced by each Butler matrix.

$$C_{harv} = S.B_o.\frac{\lambda_o^2}{4\pi}.\delta.\left|G_P^{co}(\theta_o^{1,4},0)\right|.10(\Theta_{E1}\Theta_{H1} + \Theta_{E2}\Theta_{H2}) \quad (9)$$

III. MINIATURIZED BUTLER MATRIX

The prototyped rectenna contains standards 4x4 Butler matrix with 50 Ω accesses that direct the ambient RF power captured by the antenna arrays into 4 rectifiers each. As

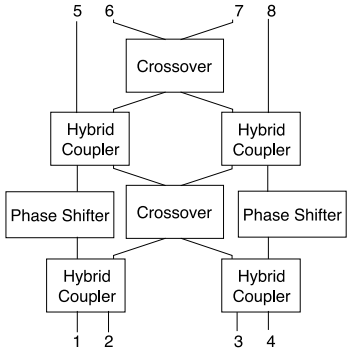

Fig. 3. Standard 4x4 Butler matrix (BM).

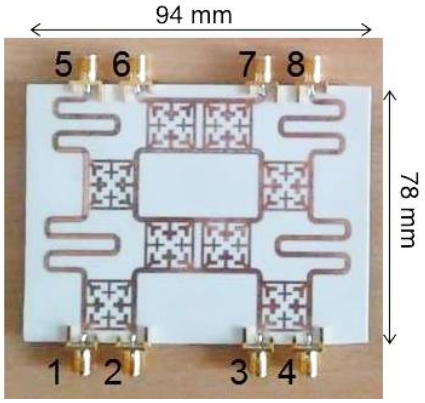

Fig. 4. Picture of the miniaturized Butler matrix.

TABLE I
PHASE SHIFTS AT OUTPUT PORTS OF THE BM AT FREQUENCY OF OPERATION

Phase	Ideal	Simulated @ 2.45 GHz	Measured @ 2.42GHz
$\varphi(S(5,1)–S(6,1)) = \beta_1$	45°	45.45°	37.20°
$\varphi(S(6,1)–S(7,1)) = \beta_1$	45°	45.48°	50.66°
$\varphi(S(7,1)–S(8,1)) = \beta_1$	45°	43.49°	40.41°
$\varphi(S(5,2)–S(6,2) = \beta_2$	-135°	-132.33°	-138.45°
$\varphi(S(6,2)$-$S(7,2)) = \beta_2$	-135°	-136.08°	-130.47°
$\varphi(S(7,2)–S(8,2)) = \beta_2$	-135°	-136.54°	-141.52°
$\varphi(S(5,3)–S(6,3)) = \beta_3$	135°	136.62°	136.58°
$\varphi(S(6,3)–S(7,3)) = \beta_3$	135°	136.10°	135.548°
$\varphi(S(7,3)–S(8,3)) = \beta_3$	135°	132.41	130.72°
$\varphi(S(5,4)–S(6,4)) = \beta_4$	-45°	-43.42°	-47.24°
$\varphi(S(6,4)–S(7,4)) = \beta_4$	-45°	-45.47°	-44.82°
$\varphi(S(7,4)–S(8,4)) = \beta_4$	-45°	-45.36°	-43.71°

shown in Figure 3, this passive beam-forming network is composed of 4 hybrid couplers, 2 crossovers and 2 phase shifters of 45°. The simulated and measured results of a Butler matrix were given in a previous work [22]. The matrix is designed in microstrip technology at the frequency 2.45 GHz. As the lengths of the couplers lines are equivalent to $\lambda_g/4$, the dimensions (without the feed lines) of this classical design were expectedly large (112x130 mm²) and needed to be reduced for practical use. The miniaturization technique used in this work consists of replacing the branch lines and through lines of the hybrid couplers by transmission lines with open end stubs [24]. The through lines and branch lines of an hybrid coupler whose electrical lengths are 90° can be seen as two lines of electrical length of 45°. Each of these lines can be transformed into one transmission line with two open ended stubs. Associating the two 45° lines, one gets through lines and branch lines with three open stubs. Low impedance stubs are usually obtained and the structure becomes rapidly not realizable, especially at 2.45 GHz. That is why, as it has been proposed in [24], the open ended stubs are transformed into two-step stubs of high and low impedance sections. Finally, the length of the through lines and the branch lines of the hybrid couplers is reduced with this method from $\lambda_g/4$ to $\lambda_g/12$ leading to a Butler matrix, shown on Figure 4, of dimensions 94 x 78 mm², which is twice smaller than the classical design. The crossovers are designed by associating two hybrid couplers and transmission lines are used as phase shifters. The advantage of this

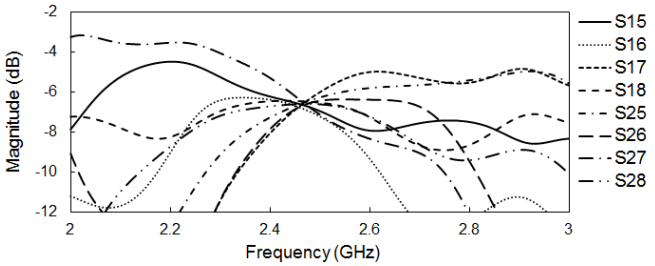

Fig. 5. Simulated amplitudes (dB) in transmission from ports 5,6,7 and 8 to ports 1 and 2 of the Butler matrix. Transmissions to ports 3 and 4 are similar to those to ports 1 and 2 due to the symmetry of the matrix.

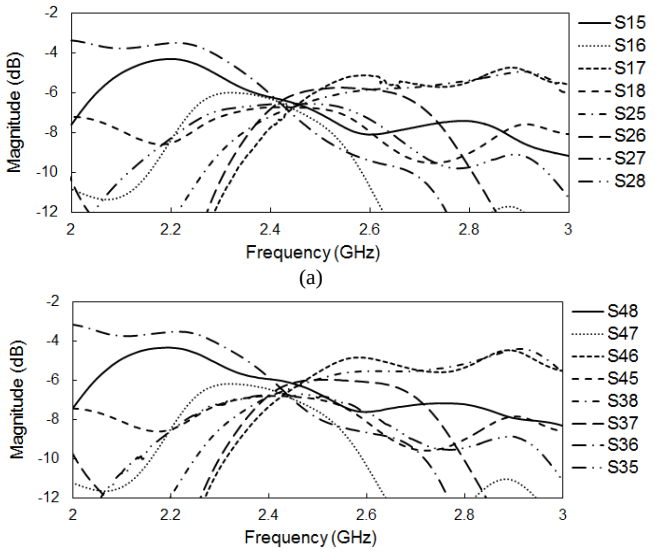

Fig. 6. Measured amplitudes (dB) in transmission from ports 5,6,7 and 8 to ports 1 and 2 (a) and to ports 3 and 4 (b) of the Butler matrix.

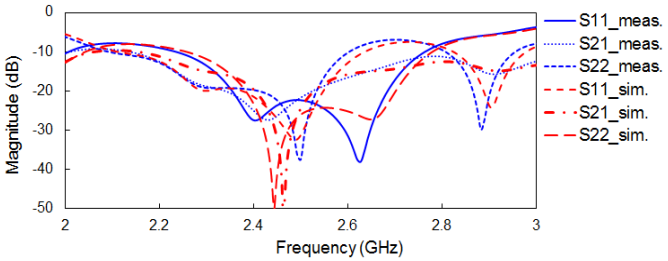

Fig. 7. Simulated and measured reflection and isolation coefficients (dB) of ports 1 and 2 of the Butler matrix.

technique is that the resulting hybrid couplers have similar insertion losses than its classical counterpart. The matrix is designed and optimized with Momentum of ADS Keysight and fabricated on the RO4003 substrate with thickness of 0.83 mm. Figure 5 gives the simulation results for the transmission magnitude from output ports 5, 6, 7 and 8 to ports 1 and 2. Figure 6 shows the measured amplitude in transmission from the output ports to the input ports. Transmissions to ports 3 and 4 are similar to those to ports 1 and 2, due to the symmetry of the Butler matrix. For this reason, only the simulation results of transmissions to ports 1 and 2 are presented here. The measured results agree well with the simulated results. The minimum experimental average insertion losses are found to be 6.61 ± 0.60 dB at

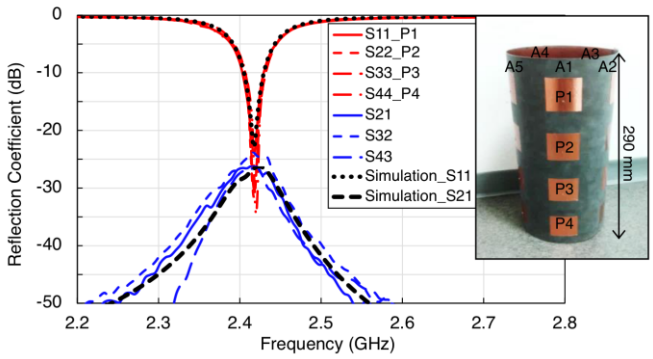

Fig. 8. Simulated and measured S-parameters (dB) of one vertical antennas array (A1) making up the total cylindrical antenna array (inside graph). The frequency of operation of the antennas is 2.42 GHz.

TABLE II
MAXIMUM GAIN IN THE ELEVATION PLANE OF THE PATCH ANTENNAS OF A1

Patch	Simulated @ 2.42 GHz Flat 1 Array	Simulated @ 2.42 GHz Bent 1 Array	Simulated @ 2.42 GHz Bent Whole Structure	Measured @ 2.42GHz Bent Whole Structure
P1	6.21 dBi	5.99 dBi	5.96 dBi	4.62 dBi
P2	5.65 dBi	5.39 dBi	5.59 dBi	4.58 dBi
P3	5.55 dBi	5.46 dBi	5.54 dBi	4.50 dBi
P4	6.18 dBi	5.96 dBi	5.67 dBi	4.42 dBi

2.42 GHz while the simulated ones are equal to 6.60 ± 0.41 at 2.45 GHz. Concerning the phase, as shown in Table I, anomalies are observed in the transmission coefficients related to ports 1 and 2 with an error reaching 7°. This is caused by a defect in the fabrication process of one side of the matrix. Otherwise, a good agreement is found with simulation for the experimental transmissions to ports 3 and 4 with a maximum phase deviation of 4.28°, only 1.8° more than in simulation. Moreover, satisfactory reflection and isolation around -20 dB are measured at ports 1 and 2 over the whole 2.4 GHz band, as shown in Figure 7.

IV. QUASI-ISOTROPIC ANTENNA ARRAYS

A cylindrical antenna array composed of 5 vertical antenna arrays (A1, A2, A3, A4, A5) is designed on a flexible substrate to fit around a pole of 13 cm diameter and obtain an isotropic radiation pattern. Each antenna array is composed of 4 square patch antennas (P1, P2, P3, P4) of 40 mm side lengths, matched to 50 Ω that are connected to the ports 5, 6, 7 and 8 of the 4x4 Butler matrix. The antennas share the same ground and are spaced apart from each other by $\lambda_o/2$ to limit the height of the prototype to 29 cm while avoiding mutual coupling effects. The diameter of the cylindrical antenna array has to be high enough so that the five antenna arrays fit with a spacing of $\lambda_o/2$ between them. This leads to a minimum diameter of 13 cm. The antenna arrays are designed and optimized for this diameter on CST Microwave Studio. It is fabricated on the flexible RO5880 substrate with thickness of 0.72 mm and relative permittivity of 2.2. As illustrated in Figure 8, the frequency of operation of the antennas is close to 2.42 GHz, similar to the frequency of operation of the Butler matrix. The experimental S11 parameters are below -

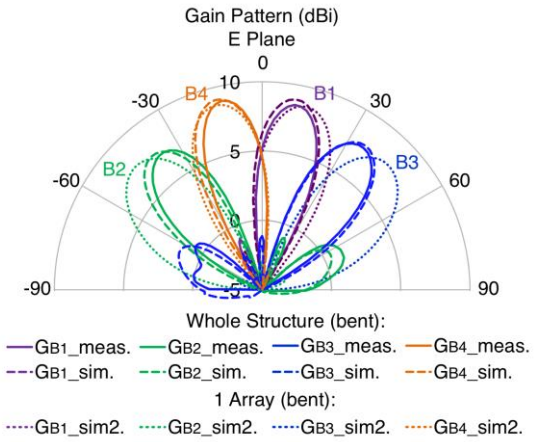

(a)

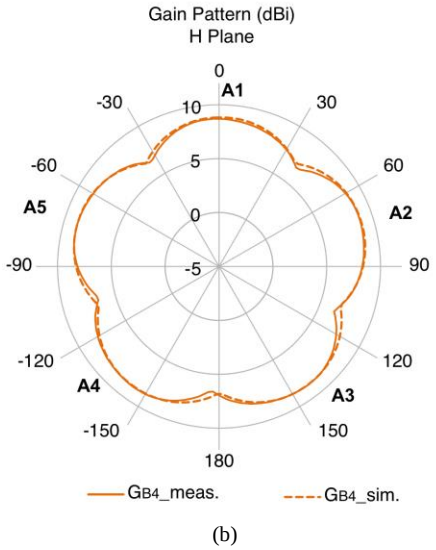

(b)

Fig. 9. Measured and simulated gain pattern (dBi) (a) of one multidirectional antenna array (A1 associated to the BM) in the E-plane, as a function of the incident angle θ (°) and (b) of beam B4 in the H-plane ($\theta = \theta_o^4$) of the whole cylindrical antenna array. f = 2.42 GHz.

23 dB when the antennas are bent, in agreement with the simulation. Moreover, the mutual coupling between antennas is below -25 dB over the whole band. As shown in Table II, the simulation of one 4-antennas array in CST gives lower maximum gains for each patch antenna when it is bent compared to when it is flat and with similar matching. This suggests that, the bending affects the radiation of patch antennas as it was reported in [25]. Nonetheless, the effect of the curvature on the gains remains low due to the slight bending. On the other hand, we can see that the presence of all the other antenna arrays hardly affects the maximum gain of each patch antenna. The realized gains are measured for the bent array in an anechoic chamber. As shown in Table II, the antennas exhibit a discrepancy in measurement around 1 dB in the maximum gain due to the fabrication tolerance and the incertitude of the measurement setup (alignment of the antenna under test and calibration). Figures 9 (a) presents the measured and simulated gain pattern in the elevation plane of one multidirectional antenna array (A1) connected to the Butler matrix with RF cables. The simulated gain magnitudes are obtained by combining the experimental co-polar gains of

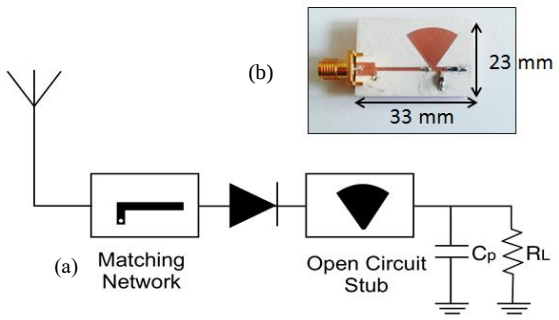

Fig. 10. (a) Topology and (b) picture of the single series diode rectifier. Cp = 2.2 nF and R_L = 5.1 kΩ.

each antenna with the experimental phase differences induced by the Butler matrix using phase shifters. A power divider is used to observe the experimental amplitudes at the matrix outputs and therefore take into consideration the insertion losses. The cable losses of 0.55 dB are also added to the simulation. A good agreement is found between measurement and simulation. Although, the cylindrical organization of the 5 antenna arrays does not affect the maximum gain, we can observe a diminution of the beams' widths in the elevation plane, in simulation, with the whole structure compared to the beams obtained with the 4-antenna array alone. This is due to the mutual coupling between the patch of the different arrays. Note also that, due to mutual coupling between the patch of the same array, the larger the scanning angles, the less directives the lobes get. Still, 4 beams gain are measured, which peak at 8.84 and 8.47 dBi for B4 and B1, and 7.52 and 7.22 dBi for B3 and B2, at the scan angles of -12°, 8°, -34 and 36° respectively. The half power beam widths of beams B4, B1, B3 and B2 of 22, 21, 26 and 26° respectively in the E-plane and 80, 72, 86 and 45° in the H-plane do not overlap, thus ensuring wide overall beam widths. Note also that the gain magnitudes of beams B1 and B2 are slightly lower than the gain of B3 and B4 due to the errors in phase shifts of the Butler matrix as mentioned in section III. Figure 9 (b) shows the gain resulting from the beams B4 of all of the 5 antenna arrays in the H-plane at $\theta = \theta_o^4$). The gain pattern of B4 is measured by associating the antenna array A1 with the Butler matrix. It is shifted each time by 72° to reproduce the gain of the other antenna arrays and the maximum gain at each azimuthal angle is taken. This results in a total constant high gain between 6 and 8.8 dBi in the H-plane. A good agreement is found between simulation and measurement. In conclusion, each antenna array can collect vertically polarized RF signals with high gain within a wide angle in their E-plane and the 5 antenna arrays offer a high gain quasi-omnidirectional radiation pattern in the H-plane. To evaluate the spatial coverage of the rectenna, the solid angle of the multidirectional array A1 is calculated by summing up the solid angles of each beam, determined by equation (4). The solid angle of the whole system made of the 5 arrays is then found to be 3.87π, that is 97% of the solid angle of a sphere. This means that the power is captured by the rectenna with a gain always higher than 4.5 dBi for 97% of all possible angles of arrival of the incoming radiation.

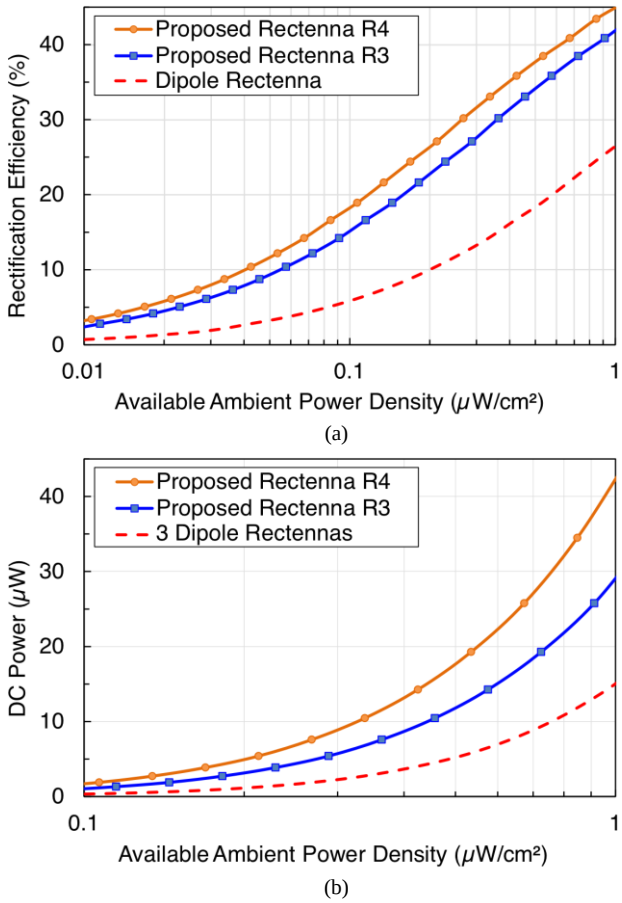

Fig. 11. Experimental (a) rectification efficiency (%) and (b) DC power (μW) of the rectifier associated to the proposed antenna array + beam-forming (R3 and R4) and associated to a dipole antenna (multiplied by 3 for the DC power) as a function of the theoritical available ambient power density (μW.cm^{-2}) at the frequency of 2.42 GHz.

V. Rectenna Measurements

A. Rectifier Characterization

Four rectifiers are connected to ports 1, 2, 3 and 4 of the Butler matrix of the demonstrator for the RF-DC conversion. As we want to harvest the ambient RF power, the single series diode configuration is selected to minimize the power consumption of the diodes. As such, the rectifier consists of a series diode, a DC-pass filter and a resistive load. The rectifying element is the Schottky diode SMS7630, and the load is chosen to be a 5.1 kΩ resistor, close to the junction resistance of the diode for an optimal DC-DC transfer [3]. A shunt capacitor of 2.2 nF acts like a DC pass filter and an open circuit stub between the diode and this filter helps in rectifying the maximum current points. A Momentum co-simulation is performed in Keysight ADS with the Large Signal S-Parameters (LSSP) simulator for the evaluation of the input impedance. A matching network is designed with a short circuit stub for an input power of -30 dBm to match the rectifier to 50 Ω. The rectifier is shown in Figure 10, and it is fabricated on the RO6002 substrate with thickness of 1.524 mm and relative permittivity of 2.94. The output DC voltage V_{DC} of the rectifier is measured across the resistive load R_L with a precision voltmeter for a RF input power P_{RF} ranging

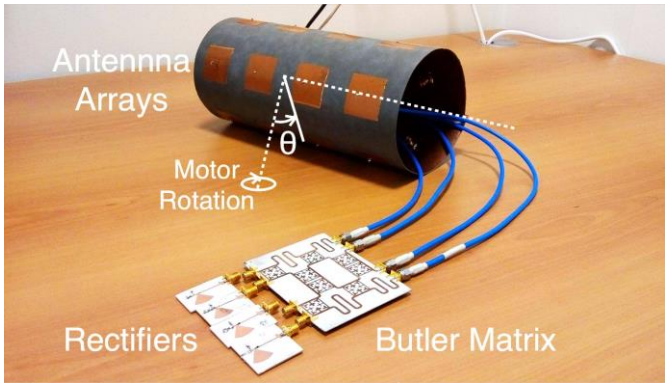

Fig. 12. Picture of the proposed rectenna with one Beam-Forming Network (BFN).

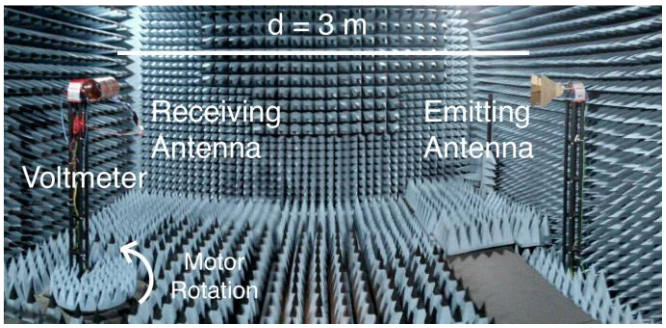

Fig. 13. Measurement setup in the anechoic chamber.

from -40 to -10 dBm at the frequency of 2.42 GHz. The rectification efficiency is then computed using

$$\eta_r = \frac{V_{DC}^2}{R_L.P_{RF}} \quad (10)$$

and plotted as a function of the available ambient RF power density calculated for different antenna gains with expression (2), as shown in Figure 11 (a). The overall rectification efficiency is given for rectifiers R4 and R3 that receive energy from the antenna array A1 and the Butler matrix with experimental maximum gains G_{B4} = 8.84 dBi and G_{B3} = 7.52 dBi respectively and for a dipole rectenna of 1.9 dBi gain. The proposed rectenna improves the rectification efficiency of a Rectenna made of an omnidirectional dipole antenna by a factor dependent on the orientation of the incoming beam and on the available incident power density. For example, under a very low ambient power density of 10 nW.cm^{-2}, the rectification efficiency of the rectifier associated with the dipole antenna can get multiplied by 3.4 (R3) or 4.6 (R4) when associated with the proposed antenna array. Figure 11 (b) compares the DC power at the rectifier outputs as a function of the available power density to the DC power provided by 3 dipole rectennas. The association of several dipoles antennas are highly limited due to the high mutual coupling between the antennas. Thus, in order to obtain an unaffected omnidirectional pattern, electric dipole antennas can only be arranged on the same vertical line with a minimum spacing equivalent to a half wavelength between the extremities of the arms of each dipole. Hence, the height of a 4 patch antenna array (29 cm) represents at best to the

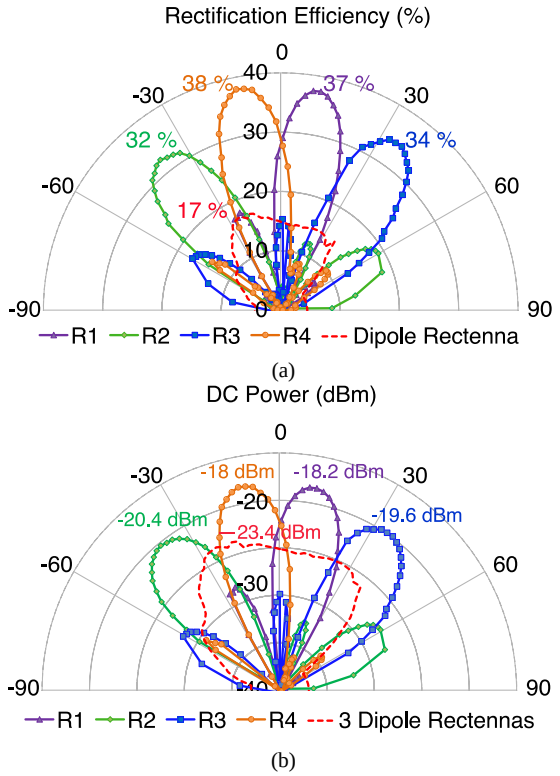

Fig. 14. Experimental (a) rectification efficiency pattern (%) and (b) DC power pattern (dBm) in the E-plane, as a function of the incident angle θ (°), of rectifiers R1, R2, R3 and R4 of one multidirectional rectenna and of a dipole rectenna. The power density and frequency of the incident radiation are 0.45 µW.cm^{-2} and 2.42 GHz, respectively.

height of an array of 3 half-wave dipoles antennas. The graph 11 (b) demonstrates that, by functioning more efficiently, rectifiers R3 and R4 produce a larger amount of DC power than 3 dipole rectennas. Actually, because the rectification efficiency varies linearly with the received RF power, the output DC power is proportional to the square of the input power. Besides, in reality, the DC combination of the output of 3 dipoles rectennas accounts for losses especially at low power levels. This result confirms that, for low input power densities, it is more advantageous to increase the gain of the antenna rather than increasing the number of rectennas, and the proposed system appears to be the only solution to obtain a full spatial coverage.

B. Rectenna Efficiency and DC Power Patterns

The DC voltage is measured at a dipole rectenna's output of 1.9 dBi maximum gain, and at the 4 rectifiers' outputs R1, R2, R3 and R4, connected to the Butler matrix and the antenna array A1 as illustrated on Figure 12. Measurement is performed in an anechoic chamber at frequency of 2.42 GHz as shown in Figure 13. A RF signal generator, placed outside of the chamber and transmitting a power of 20 dBm, is connected to an emitting horn antenna of 8.6 dBi gain, 3 m away from the receiving rectenna. A horn antenna with a well-known gain (8.4 dBi) is first placed at the same location than the rectenna and the power received is measured through a spectrum analyzer. From this, the incident power density is estimated with equation (2) to be 0.45 µW.cm^{-2} at the system

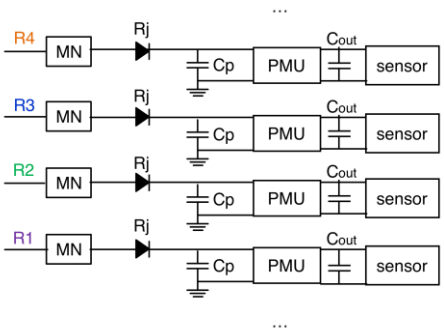

Fig. 15. DC power management of the proposed rectenna.

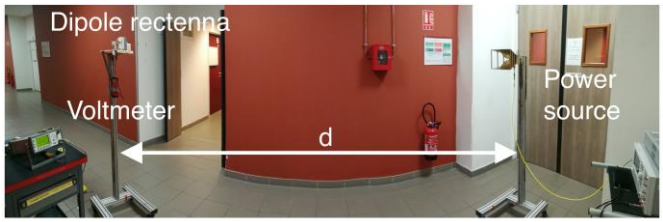

Fig. 16. Measurement set-up in the corridor.

level. Then, placed in front of the emitting antenna, the rectenna is rotated with a motor over a 180° angle in order to vary the angle of incidence θ of the RF radiation on the rectenna in the E-plane as shown in Figure 13. The DC voltage is measured every 2° at the rectifiers output inside the anechoic chamber with a voltmeter. Then, from a characterization of the rectifier with a RF signal generator, the RF input powers corresponding to each values of the measured DC voltage are retrieved. From the input power values, the rectification efficiency is computed for every angle with equation (10). Figure 14 (a) shows the rectification efficiency pattern. A similar pattern as for the gain pattern can be observed: 4 narrow beams are converted with high efficiency related to the different rectifiers. As expected from Figure 11 (a), the maximum efficiency is improved from 17% with the dipole rectenna up to 38 % with R4, 37 % with R1, 34% with R3 and to 32% with R2. Furthermore, the minimum rectification efficiency of the system in a 100° angle range is 23 %. Since the solid angle of the rectenna is 3.87π, the harvesting capability is found with equation (3) to be 36.8π %.steradian at 0.45 µW.cm^{-2} whereas the half wave dipole rectenna has a solid angle of 2.06π and a harvesting capability of 8.8π %.steradian. Figure 14 (b) illustrates the DC power pattern in dBm measured in the E-plane of the system. It is compared to the DC power pattern of 3 dipole rectennas: the DC power is measured in the E-plane of the dipole rectenna output of 1.9 dBi maximum gain and multiplied by 3. The 3 dipole rectennas provide a maximum DC power of -23.4 dBm (4.6 µW) which corresponds approximately to the minimum amount of power delivered by the proposed system in the 100° range of angles. Otherwise, the proposed rectenna offers maximum DC powers from -19.65 dBm (10.8 µW) to -18 dBm (15.8 µW), depending on the orientation of the receiving beam, which yields 2 to 3 times more power than 3 dipole rectennas.

C. Rectenna Sensitivity

The power supply of a sensor requires the provision of a sufficient DC voltage at a specific fixed value. Because

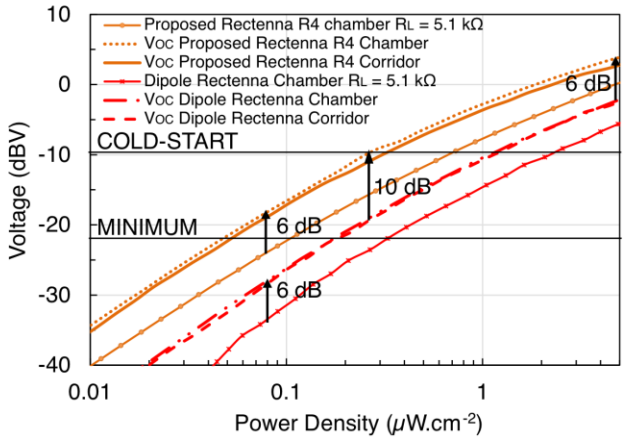

Fig. 17. Experimental DC voltage (dBV) at the output of the rectifier (open-circuit and R_L=5.1kΩ) associated to the proposed antenna array + beam-forning (R4) and associated to a dipole antenna, as a function of the power density (µW.cm^{-2}). f = 2.42 GHz.

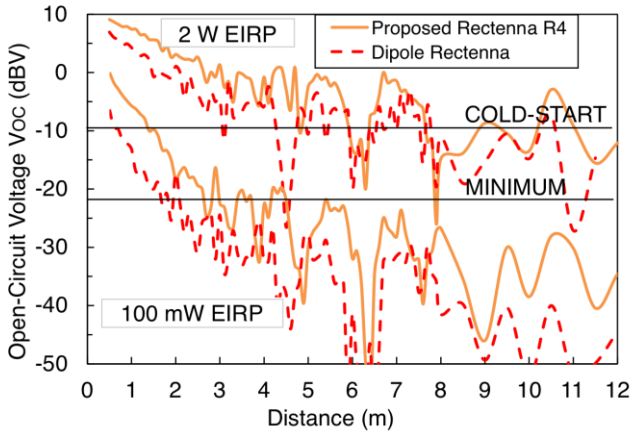

Fig. 18. Experimental open-circuit voltage (dBV) at the output of the rectifier associated to the proposed antenna array + beam-forning (R4) and associated to a dipole antenna as a function of the distance (m) under 2 FCC-regulated emitting powers of 100 mW and 2W . f=2.42GHz.

ambient RF energy density is very low and time varying, the output DC voltage of a rectenna is not constant over time and generally too weak to directly drive a sensor. For this reason, a DC-DC converter is necessary at the rectifier output to boost and regulate the DC voltage. For very low power densities, an ultra-low power boost converter (Power Management Unit (PMU)) such as BQ25504 from Texas Instrument (TI) can be adopted to store energy in a capacitor and drive a low power sensor operated in a low duty cycle mode. The boost converter performs a "Maximum Power Point Tracking" (MPPT) so that the rectifier transfers the maximum DC power at any instant. For this, the DC-DC converter frequently samples the harvester open circuit voltage and sets its input voltage to a configurable optimal portion of it. At low power levels, the DC power transfer to the boost converter is optimal when the converter is seen as a load equal to R_j [3], that is when the input voltage of the boost converter is a half of the open circuit voltage of the rectifier. For this reason, the MPP ratio generally has to be fixed at 0.5. The boost converter needs a cold-start open-circuit voltage of 330 mV to start charging the capacitor and then works with typical input voltages as low as 130 mV and

TABLE III

COMPARISON OF THE PROPOSED RECTENNA WITH STATE-OF-THE-ART RECTENNAS FOR AMBIENT RF ENERGY HARVESTING

Reference	Frequency (GHz)	Maximum Relative Effective Aperture A	Maximum Efficiency @ 1 $\mu W.cm^{-2}$ $\eta_{R_{max}}$ (%)	Half-Power Beam width in the E plane Θ_E (°)	Half-Power Beam width in the H plane Θ_H (°)	Solid Angle Ω (steradian)	**Harvesting Capability @ 1 $\mu W.cm^{-2}$ C_{harv} (%.steradian)**	Dimensions (mm^3)
[14] 2013	1.8 and 2.1 dual band	1.7 λ_o^2	56	15	110	0.16 π	**2.2 π**	300 x 380 x 1.6
[6] 2012	2.4 single band	0.57 λ_o^2	70	30	60	0.17 π	**3.1π**	110 x 90 x 20
[7] 2010	2.4 single band	0.47 λ_o^2	38.2 @1.5 $\mu W.cm^{-2}$	65 (typical)	65 (typical)	0.41 π	**3.9 π @1.5 $\mu W.cm^{-2}$**	34 x 34 x 7
[15] 2015	1.8 – 2.1 broadband	0.14 λ_o^2	47	45	109	0.48 π	**5.6 π**	70 x 70 x13.2
[18] 2017	0.9-1.8-2.6 multiband	0.10 λ_o^2	41	108	81	0.85 π	**8.7 π**	110 x 110 x0.37
[21] 2017	2.4 single band	0.74 λ_o^2	45	center lobes :30 side lobes: 40	center lobes: 80 side lobes: 80 (assumed)	1.1 π	**12.2 π**	60 x 100 x ?
[11] 2013	0.9 and 2.4 dual band	0.12 λ_o^2	37	78 (typical)	omnidirectional (typical)	2.36 π	**21.8 π**	60 x 60 x 60
[10] 2017	1.8 single band	0.16 λ_o^2	42.5	90	omnidirectional (typical)	2.64 π	**28 π**	45 x 45 x 0.8
This Work	**2.4 single band**	**0.62 λ_o^2**	**45**	**center lobes : 22 side lobes: 26**	**center lobes : 80 side lobes: 86**	**3.87 π**	**43.6 π**	**290 x 130^2 π**

down to 80 mV. The major challenge in the design of an ambient RF harvester is to make sure that the rectifier meets the cold-start requirement at the low ambient power levels.

The proposed demonstrator is composed of several rectifiers collecting energy, or not, depending on the incident angle of the harvested radiation. Hence, the optimal solution for zero or negligible power losses is to assign one DC-DC converter to each rectifier so that they function independently [1], as shown in Figure 15. Because each rectifier is receiving more energy than the case of a dipole antenna thanks to the high gain antennas, the proposed system enables the boost converter to cold-start more easily than a rectenna with an omnidirectional antenna.

To demonstrate the increase in sensitivty, the open-circuit is measured at the ouput of the rectifier R4 and of the rectifier associated to the dipole antenna, the rectennas are positionned such that they receive the RF power with maximum gain. The same measurement setup as in section V.B is installed but an amplifier with a 30 dB gain is added between the RF generator and the emitting horn antenna to generate power densities from 0.01 to 5 $\mu W.cm^{-2}$. The measurement is performed in an anechoic chamber and in a corridor with a 3m distance between the emitting antenna and the rectenna under test, as shown in Figure 16. Simular results are obtained in the anechoic chamber and in the corridor as depicted in Figure 17. This shows that when radio waves are coming from only one direction at a time, which is achieved with the directive emitting antenna, the multipath propagation does not benefit the omnidirectional dipole antenna. At low power levels, the open-circuit voltage is verified to be twice (+6dB) the voltage across a load of 5.1 kΩ and it increases of up to 10 dB (which corresponds to a multiplication by a factor higher than 3) with the proposed rectenna compared to a dipole rectenna. This increase in open-circuit voltage allows the proposed rectenna to reach the cold-start requirement of the boost converter for a power density of 0.26 instead of 1.19 $\mu W.cm^{-2}$ with a rectenna made up of a dipole antenna.

To illustrate the improvement in sensitivity, the RF power source is fixed to the maximum power levels at 2.4 GHz allowed in Europe (2W EIRP) and in France (100mW EIRP) and the distance between the rectennas and the emittig antenna is varied. Figure 18 shows the measured open-circuit voltages as a function of the distance. The minimum distances from the 100 mW EIRP power source for the rectenna to deliver the required cold-start open-circuit voltage and the minimum voltage of the boost converter are measured to be 1.5 (1.83m in theory) and 4.5m (4.48m in theory) with the proposed system while these distances with the dipole antenna are 0.6 (0.83m in theory) and 1.75m (2m in theory). As predicted by Figure 17, the difference between the open-circuit voltage (and thus the minimum distance to activate a DC-DC converter) of the proposed rectenna and the rectenna made up of a dipole reduces when the power levels increase. That is why the improvement of the sensitivty with the 2W EIRP power source is not as appreciable as with the 100mW EIRP power source. Nonetheless, these results illustrate the utility of the proposed system when low power densities are available such as in ambient scenarios. Note that the rectenna sensitivity can be largely improve when harvesting lower frequency bands at the expense of greater dimensions.

VI. PERFORMANCE COMPARISON

Table III gives a comparison between the state-of-the-art rectennas for ambient RF energy harvesting and the proposed demonstrator. The maximum rectification efficiency at a power density of 1 $\mu W.cm^{-2}$ and the half power beam widths

(HPBW) in the E and H-planes are given for each rectenna. When the HPBWs are not available in those papers, typical values are taken from theoretical radiations patterns. From these, the solid angles are computed with equations (4) or (5). It can be seen that our rectenna has the harvesting pattern that is the closest to an isotropic pattern, with a solid angle of 3.87π close to the solid angle of a sphere, due to a high number of antennas, and has a high rectification efficiency at low power density, which is due to the high effective antenna arrays' apertures. Note that, by working at lower frequency than 2.4 GHz, higher effective aperture could be obtained and hence higher efficiency. It is clear that the higher the effective antenna aperture is, the higher the rectification efficiency becomes. However, in general, increasing the effective apertures leads to a higher sensitivity to the energy source location and to low harvesting capability, which is avoided with our rectenna. Hence, while the maximum harvesting capability at 1 $\mu W.cm^{-2}$ found in the literature does not exceed 28π %.steradian, it reaches 43.6π %.steradian for the proposed demonstrator. It can also be noted that multi-tone rectenna efficiency can be improved thanks to the presence of several radio waves of different frequencies [14], [17]. Besides, implementing low loss matching networks [6] as well as an enhanced rectifier configuration [15] helps in achieving higher efficiencies. Hence, the possible prospects of this work are to combine multiband rectification and beam forming techniques and to increase the rectifier performance. Finally, the dimensions of our rectenna can be reduced by improving the effective aperture efficiency of the antennas that is the ratio between effective aperture and physical size of the antennas/antenna arrays.

VII. Conclusion

This paper discusses a novel approach to evaluate the performance of ambient energy harvesting rectennas by exploiting the multi-directionality of antenna arrays associated with beam-forming networks. A miniaturized 4x4 Butler matrix and a cylindrical antenna array have been designed to experimentally show that the high gain and wide coverage of antenna arrays coupled with Butler matrices improve the harvesting capability compared to a rectenna made of an omnidirectional dipole antenna. It has also been shown that the system helps in fulfilling the cold-start requirement of a Power Management Unit: with high gain antennas, each rectifier delivers enough DC voltage for the cold-start under lower ambient power density levels than with a rectenna made of a simple omnidirectional dipole antenna. Finally, the highest harvesting capability found in the literature so far is reported to be 28π %.steradian at 1 $\mu W.cm^{-2}$ while the harvesting capability of the proposed demonstrator is 43.6π %.steradian.

Acknowledgment

The authors would like to thank the ANR for its sponsorship in the project "Stick it" and the European project "CONVERGENCE". The authors are also grateful to Nicolas Corrao and Antoine Pisa for the fabrication of the circuits and their technical support.

References

[1] M. Pinuela, P. D. Mitcheson, and S. Lucyszyn, "Ambient RF Energy Harvesting in Urban and Semi-Urban Environments," *IEEE Trans. Microw. Theory Tech.*, vol. 61, no. 7, pp. 2715–2726, Jul. 2013.

[2] H. J. Visser, A. C. F. Reniers, and J. A. C. Theeuwes, "Ambient RF Energy Scavenging: GSM and WLAN Power Density Measurements," in *2008 38th European Microwave Conference*, 2008, pp. 721–724.

[3] S. Hemour, Y. Zhao, C.H.P. Lorenz, D. Houssameddine, Y. Gui, C-M Hu, K. Wu, "Towards Low-Power High-Efficiency RF and Microwave Energy Harvesting," *IEEE Trans. Microw. Theory Tech.*, vol. 62, no. 4, pp. 965–976, Apr. 2014.

[4] C. H. P. Lorenz, S. Hemour, W. Li, Y. Xie, J. Gauthier, P. Fay, K. Wu, "Breaking the Efficiency Barrier for Ambient Microwave Power Harvesting With Heterojunction Backward Tunnel Diodes," *IEEE Trans. Microw. Theory Tech.*, vol. 63, no. 12, pp. 4544–4555, Dec. 2015.

[5] Z. Popović, E. A. Falkenstein, D. Costinett and R. Zane, "Low-Power Far-Field Wireless Powering for Wireless Sensors," in *Proceedings of the IEEE*, vol. 101, no. 6, pp. 1397-1409, June 2013.

[6] H. Sun, Y. x Guo, M. He, and Z. Zhong, "Design of a High-Efficiency 2.45-GHz Rctenna for Low-Input-Power Energy Harvesting," *IEEE Antennas Wirel. Propag. Lett.*, vol. 11, pp. 929–932, 2012.

[7] A. Georgiadis, G. V. Andia, and A. Collado, "Rectenna design and optimization using reciprocity theory and harmonic balance analysis for electromagnetic (EM) energy harvesting," *IEEE Antennas Wirel. Propag. Lett.*, vol. 9, pp. 444–446, 2010.

[8] U. Olgun, C. C. Chen, and J. L. Volakis, "Investigation of Rectenna Array Configurations for Enhanced RF Power Harvesting," *IEEE Antennas Wirel. Propag. Lett.*, vol. 10, pp. 262–265, 2011

[9] Z. Popović et al., "Scalable RF Energy Harvesting," in IEEE Transactions on Microwave Theory and Techniques, vol. 62, no. 4, pp. 1046-1056, April 2014.

[10] M. Zeng, A. S. Andrenko, X. Liu, Z. Li and H. Z. Tan, "A Compact Fractal Loop Rectenna for RF Energy Harvesting," in *IEEE Antennas and Wireless Propagation Letters*, vol. 16, pp. 2424-2427, 2017.

[11] K. Niotaki, S. Kim, S. Jeong, A. Collado, A. Georgiadis, and M. M. Tentzeris, "A Compact Dual-Band Rectenna Using Slot-Loaded Dual Band Folded Dipole Antenna," *IEEE Antennas Wirel. Propag. Lett.*, vol. 12, pp. 1634–1637, 2013.

[12] Y.-H. Suh and K. Chang, "A high-efficiency dual-frequency rectenna for 2.45- and 5.8-GHz wireless power transmission," *IEEE Trans. Microw. Theory Tech.*, vol. 50, no. 7, pp. 1784–1789, Jul. 2002.

[13] H. Sun, Y. x Guo, M. He, and Z. Zhong, "A Dual-Band Rectenna Using Broadband Yagi Antenna Array for Ambient RF Power Harvesting," *IEEE Antennas Wirel. Propag. Lett.*, vol. 12, pp. 918–921, 2013.

[14] C. Song, Y. Huang, J. Zhou, J. Zhang, S. Yuan, and P. Carter, "A High-Efficiency Broadband Rectenna for Ambient Wireless Energy Harvesting," *IEEE Trans. Antennas Propag.*, vol. 63, no. 8, pp. 3486–3495, Aug. 2015.

[15] A. Costanzo, A. Romani, D. Masotti, N. Arbizzani, and V. Rizzoli, "RF/baseband co-design of switching receivers for multiband microwave energy harvesting," *Sens. Actuators Phys.*, vol. 179, pp. 158–168, June 2012.

[16] C. Song *et al*., "A Novel Six-Band Dual CP Rectenna Using Improved Impedance Matching Technique for Ambient RF Energy Harvesting," in *IEEE Transactions on Antennas and Propagation*, vol. 64, no. 7, pp. 3160-3171, July 2016.

[17] V. Palazzi *et al*., "A Novel Ultra-Lightweight Multiband Rectenna on Paper for RF Energy Harvesting in the Next Generation LTE Bands," in *IEEE Transactions on Microwave Theory and Techniques*, vol. PP, no. 99, pp. 1-14.

[18] C. H. P. Lorenz, S. Hemour, W. Liu, A. Badel, F. Formosa, and K. Wu, "Hybrid Power Harvesting for Increased Power Conversion Efficiency," *IEEE Microw. Wirel. Compon. Lett.*, vol. 25, no. 10, pp. 687–689, Oct. 2015.

[19] J. Kimionis, M. Isakov, B. S. Koh, A. Georgiadis, and M. M. Tentzeris, "3D-Printed Origami Packaging With Inkjet-Printed Antennas for RF Harvesting Sensors," *IEEE Trans. Microw. Theory Tech.*, vol. 63, no. 12, pp. 4521–4532, décembre 2015.

[20] S. Shen, C. Y. Chiu and R. D. Murch, "Multiport Pixel Rectenna for Ambient RF Energy Harvesting," in *IEEE Transactions on Antennas and Propagation*, vol. 66, no. 2, pp. 644-656, Feb. 2018.

[21] D. J. Lee, S. J. Lee, I. J. Hwang, W. S. Lee and J. W. Yu, "Hybrid Power Combining Rectenna Array for Wide Incident Angle Coverage in RF Energy Transfer," in *IEEE Transactions on Microwave Theory and Techniques*, vol. 65, no. 9, pp. 3409-3418, Sept. 2017.
[22] E. Vandelle, P. L. Doan, D.H.N. Bui, T.P. Vuong, G. Ardila, K. Wu, S. Hemour, "High gain isotropic rectenna," in *2017 IEEE Wireless Power Transfer Conference (WPTC)*, 2017, pp. 1–4.
[23] C. Balanis, *Antenna Theory, Analysis, and Design*, 4th ed. Wiley, 2016.
[24] I. Sakagami, M. Haga, and T. Munehiro, "Reduced branch-line coupler using eight two-step stubs," *Antennas Propag. IEEE Proc. - Microw.*, vol. 146, no. 6, pp. 455–460, décembre 1999.
[25] D. Ferreira, P. Pires, R. Rodrigues and R. F. S. Caldeirinha, "Wearable Textile Antennas: Examining the effect of bending on their performance.," in *IEEE Antennas and Propagation Magazine*, vol. 59, no. 3, pp. 54-59, June 2017.

Erika Vandelle (S'16) received the B.S degree in physics from the University Grenoble Alpes, Grenoble, France in 2014 and the M.S degree in optics, optoelectronics and microwaves engineering from the Grenoble Institute of Technology, Grenoble, France in 2016. She is currently pursuing the Ph.D degree at the University of Grenoble Alpes, Grenoble, France. Her current research interests include electromagnetic and multi-source energy harvesting and printed antennas. Ms.Vandelle was the recipient of the IEEE WPTC2017 Best Paper Award.

Do Hanh Ngan Bui (S'14**)** received the M.Sc, degree in microwaves from the Grenoble Institute of Technology (INPG), Grenoble, France in 2009 and the Ph.D. degree in radiofrequency from the University Grenoble Alpes, Grenoble, France in 2017. Since then, she has been working as researcher at the IMEP-LAHC laboratory, Grenoble, France. Her research interest is in the domain of energy harvesting and printed electronics.

Tan-Phu Vuong received the Ph.D. degree in electrical engineering from the Institut National Polytechnique (INP), Toulouse, France, in 1999. From September 2001 to September 2008, he was an Associate Professor in microwave and wireless systems at the ESISAR. His research interests include modeling of passive RF and millimeter wave. Currently, his research activities include Air-filled SIW, Metamaterial, Electronic printed and Design of small antennas and printed antennas for mobile, RFID and UWB systems. Since September 2008, he is a Professor in microwave and wireless systems at the PHELMA, INPG in France.
Dr. Vuong supervised 30 PhD theses, and authored/co-authored 42 scientific papers in international journals and more than 220 scientific communications in international refereed conferences. He is a member of several review committees and scientific societies. He has been managing ten research projects between companies and his laboratory. He was VP chapter of the IEEE French Section from 2010 to 2013.

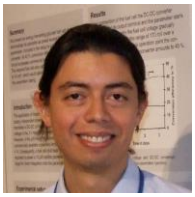

Gustavo Ardila received his BS in electronic engineering and physics from the University of Andes, Colombia in 2002 and 2003, respectively, and his MS in microelectronic and microsystems circuit conception from the National Institute of Applied Science, Toulouse, France in 2004. He received his PhD degree in Electrical Engineering in 2008 from the Paul Sabatier University in Toulouse. After a postdoctoral position in LAAS-CNRS, in 2009 he became Associate Professor at the Grenoble Alpes University and researcher at IMEP-LAHC, Grenoble, France. His current research interest is energy harvesting technologies, in particular MEMS and NEMS design, development and characterization, especially for mechanical energy harvesters and sensors but also in relation to multi-source energy harvesting (RF, solar, etc.).

Ke Wu (M'87-SM'92-F'01) received the B.Sc. degree (with distinction) in radio engineering from the Nanjing Institute of Technology (now Southeast University), China, in 1982 and the D.E.A. and Ph.D. degrees in optics, optoelectronics, and microwave engineering (with distinction) from the Institut National Polytechnique de Grenoble (INPG) and University of Grenoble, France, in 1984 and 1987, respectively.
Dr. Wu is a Professor of electrical engineering, and NSERC-Huawei Industrial Research Chair in Future Wireless Technologies with the Polytechnique Montréal (University of Montreal), QC, Canada. He has been the Director of the Poly-Grames Research Center. He was the founding Director of the Center for Radiofrequency Electronics Research of Quebec (Regroupement stratégique of FRQNT) and Tier-I Canada Research Chair in RF and millimeter-wave engineering. Currently, he is also with the School of Information Science and Engineering, Ningbo University, on leave from his home institution, leading a special 5G and future wireless research program there. He has held guest, visiting, and honorary professorships with many universities around the world. He has authored or co-authored over 1200 referred papers and a number of books/book chapters. He has filed more than 50 patents. His current research interests involve substrate integrated circuits and systems, antenna arrays, field theory and joint field/circuit modeling, ultra-fast interconnects, wireless power transmission and harvesting, and MHz-through-THz technologies and transceivers for wireless sensors and systems as well as biomedical applications. He is also interested in the modeling and design of microwave and terahertz photonic circuits and systems.
Dr. Wu is a Fellow of the Canadian Academy of Engineering (CAE) and of the Royal Society of Canada (The Canadian Academy of the Sciences and Humanities). He is a Member of Electromagnetics Academy, Sigma Xi, URSI, and IEEE-Eta Kappa Nu (IEEE-HKN). He has held key positions in and has served on various panels and international committees including the chair of Technical Program Committees, International Steering Committees, and international conferences/symposia. In particular, he was the General Chair of the 2012 IEEE Microwave Theory and Techniques (IEEE MTT-S) International Microwave Symposium (IMS). He has served on the Editorial/Review Boards of many technical journals, transactions, proceedings and letters as well as scientific encyclopedia including Editor and Guest Editor. He was the Chair of the joint IEEE Montreal chapters of MTT-S/AP-S/LEOS and then the restructured IEEE MTT-S Montreal Chapter, Canada. He has served IEEE MTT-S and Administrative Committee (AdCom) as Chair of the IEEE MTT-S Transnational Committee, Member and Geographic Activities (MGA) Committee, Technical Coordinating Committee (TCC) and 2016 IEEE MTT-S President among many other AdCom functions. He was an IEEE MTT-S Distinguished Microwave Lecturer (2009-2011). Dr. Wu is the inaugural representative of North America as a Member of the European Microwave Association (EuMA) General Assembly. He was the recipient of many awards and prizes including the first IEEE MTT-S Outstanding Young Engineer Award, the 2004 Fessenden Medal of the IEEE Canada, the 2009 Thomas W. Eadie Medal of the Royal Society of Canada, the Queen Elizabeth II Diamond Jubilee Medal in 2013, the 2013 FCCP Education Foundation Award of Merit, the 2014 IEEE MTT-S Microwave Application Award, the 2014 Marie-Victorin Prize (Prix du Quebec - the highest distinction of Québec in the natural sciences and engineering), the 2015 Prix d'Excellence en Recherche et Innovation of Polytechnique Montréal, and the 2015 IEEE Montreal Section Gold Medal of Achievement.

Simon Hemour (S'08–M'11–SM'16) received the B.S. degree in electrical engineering from the University of Grenoble Alpes, Grenoble, France, in 2004, and the M.S. and Ph.D. degrees in optics, optoelectronics, and microwave engineering from the Grenoble Institute of Technology, Grenoble, France, in 2006 and 2010, respectively. In 2003, he was with the European Organization for Nuclear Research, Geneva, Switzerland, as a member of the Instrumentation Department, where he was involved in ATLAS experiment

on the Large Hadron Collider. From 2006 to 2007, he was a Research Assistant with the Pidstryhach Institute of Applied Problems of Mechanics and Mathematics, National Academy of Science of Ukraine, Lviv, Ukraine. In 2007, he joined the IMEP-LAHC MINATEC Laboratory, Grenoble, France. From 2011 to 2015, he was with the Poly-Grames Research Center, École Polytechnique de Montréal, Montréal, QC, Canada, where he was leading the Wireless Power Transmission and Harvesting Research Group. He joined the Universite de Bordeaux, Bordeaux, France, in 2015, where he is currently an Associate Professor, and he leads research in wireless micro energy solutions for IoT and biomedical applications. His current research interests include wireless power transfer and hybrid energy harvesting, backscattering, nonlinear devices, innovative RF measurements, RF interferometry, low power microwave, and millimeterwave conversion circuits, development of RF transponders and sensors for wireless systems and biomedical applications.

Dr. Hemour is a member of the IEEE MTT-26 Wireless Energy Transfer and Conversion Technical Committee and of the IEEE MTT-10 Biological effect and medical application Technical Committee. He was the TPC chair of the 2018 Wireless Power Transfer Conference. He has served as guest editor for IEEE Transactions on Microwave Theory and Techniques, as well as for the IEEE Journal of Electromagnetics, RF and Microwaves in Medicine and Biology.